High-Fidelity Monte Carlo Simulation of Gamma-Ray Shielding Efficiency for Nuclear Security Applications Using Geant4 Toolset

Yurii Zabulonov[1], Tetiana Nosenko[2], Vitalina Lulianova[1] and Yevheniia Anpilova[3,4]
[1]*Department of Nuclear-Physical Technologies, State Institution "The Institute of Environmental Geochemistry of National Academy of Sciences of Ukraine", Academician Palladin Avenue 34a, 03142 Kyiv, Ukraine*
[2]*Department of Computer Science, Faculty of Information Technology and Mathematics, Borys Grinchenko Kyiv Metropolitan University, Levka Lukyanenka Str. 13-B, 04212 Kyiv, Ukraine*
[3]*Department of Computation Hydrosystems, Helmholtz Centre for Environmental Research GmbH, Permoser Str. 15, 04318 Leipzig, Germany*
[4]*Department of Natural Resources, Institute of Telecommunications and Global Information Space of the National Academy of Sciences of Ukraine, Chokolivskiy Bulv. 13, 03186 Kyiv, Ukraine*
1952zyl@gmail.com, t.nosenko@kubg.edu.ua, igns@ukr.net, yevheniia.anpilovat@ufz.de

Keywords: Monte Carlo Simulation, Geant4, Radiation Shielding, Buildup Factor, Nuclear Security, Special Nuclear Materials.

Abstract: The development of AI-driven radiation detection systems is hindered by the lack of high-fidelity data representing complex shielding scenarios. Most existing datasets rely on simplified exponential attenuation models, ignoring stochastic scattering effects. This study challenges this approach by presenting a Geant4-based high-fidelity simulation of gamma-ray transport for Special Nuclear Materials (^{239}Pu). While high-Z shielding (Lead) demonstrated predictable exponential attenuation (μ-validation error < 1.2%), our results reveal a critical anomaly in low-Z shielding (Polyethylene). We observed a significant non-monotonic "buildup effect" where the detected photon intensity increases by ~25-40% with shielding thickness up to 4 cm, effectively turning the shield into a scattering amplifier. This finding proves that "naive" synthetic data generation is insufficient for training robust AI models. The discovered spectral distortion mechanism is crucial for identifying SNM concealed behind common construction materials, offering a new physical baseline for "data-centric" nuclear security systems. Furthermore, this study underscores the necessity of accurately simulating the detector response and the full scattering history to prevent sim-to-real discrepancies when deploying neural networks in real-world environments. Incorporating these buildup anomalies into training datasets can significantly improve signal-to-noise ratio interpretation and reduce false negative rates in automated scanning applications.

1 INTRODUCTION

The illicit trafficking of radioactive materials and the potential deployment of Radiological Dispersal Devices (RDDs) necessitate the development of advanced radiation detection systems capable of rapid and reliable isotope identification [1]. While gamma-ray spectroscopy is a well-established technique, its effectiveness is severely compromised when sources are concealed within shielding containers. The spectral signature of a radioisotope is not static; it is a complex function of the source energy, shielding geometry, and the atomic number (Z) of the intervening material [2].

A critical limitation in developing next-generation identification algorithms, particularly those based on Deep Learning, is the scarcity of annotated experimental data involving Special Nuclear Materials like ^{239}Pu. Experimental campaigns with SNM are logistically prohibitive and constrained by safety regulations. Consequently, there is a growing reliance on synthetic data generation. However, simplified analytical models often neglect stochastic phenomena such as multiple scattering and secondary particle generation, leading to the "sim-to-real" gap [3].

This paper presents a high-fidelity simulation study using the Geant4 toolkit to characterize the shielding efficiency and spectral distortion effects of

Lead and Polyethylene. We specifically investigate the buildup factor anomaly for low-energy sources, providing a physical validation for the use of synthetic data in training robust AI detection systems.

Scientific Novelty.

- Unlike standard attenuation models used in many radiation datasets, we demonstrate that for Low-Z materials (Polyethylene) and Low-E sources (^{239}Pu), the shielding efficiency is negative. We identified a critical "buildup region" (0-5 cm) where the scattering flux dominates over absorption, causing a signal amplification of up to 40%.
- We show that simplified synthetic data generators (which assume exponential decay) fail to capture these scattering artifacts. Our Geant4-based Digital Twin proves that excluding the leads to spectrally distorted datasets that could render AI detection algorithms blind to SNM concealed behind light construction materials.

The aim of this study is to develop and verify a high-fidelity Geant4-based Digital Twin to investigate the interaction of SNM gamma radiation with composite shields and to analyze the impact of scattering buildup effects on spectral characteristics. To achieve this aim, the following objectives were set:

- To develop a simulation pipeline using precise physics lists (QGSP_BIC_HP) for photon transport modeling.
- To validate the model against NIST XCOM benchmark data.
- To conduct a comparative analysis of shielding efficiency for High-Z (Lead) and Low-Z (Polyethylene) materials.
- To quantify the buildup factor anomaly for ^{239}Pu in polyethylene, identifying conditions where shielding leads to signal amplification.

2 RELATED WORK

The challenge of detecting shielded radioactive sources has been extensively studied in the context of nuclear security and border monitoring. This involves identifying radioactive elements in the environment and assessing radiological hazards [1], [4]-[7]. The fundamental principles of gamma-ray spectroscopy and shielding physics are well-codified by Knoll [8], who highlights the difficulty of identifying low-energy emitters like ^{239}Pu in the presence of background radiation and Compton scattering artifacts.

2.1 Monte Carlo Simulations in Nuclear Security

Given the practical constraints of handling SNM, Monte Carlo (MC) simulations have become the de facto standard for generating training data and testing detection algorithms. The Geant4 toolkit [9] has been widely validated against experimental benchmarks. For instance, recent works [10] demonstrated Geant4's precision in modeling NaI (Tl) detector responses. However, many simulation studies focus on simplified "narrow-beam" geometries that adhere strictly to the Beer-Lambert attenuation law. Such approximations often fail to capture the complex "broad-beam" scattering environments typical of real-world cargo scanning, where the buildup factor becomes significant.

2.2 Shielding Materials and Buildup Factors

The physics of radiation transport in composite materials is critical for accurate modeling. The NIST XCOM database [11] provides standard reference data for photon cross-sections. However, as noted by Hubbell [12], the buildup factor-which corrects for scattered photons reaching the detector-is highly sensitive to the atomic number (Z) of the shield. While high-Z materials like Lead act as near-perfect absorbers, low-Z materials (water, polyethylene, concrete) function as scattering media. Research by Singh et al. [13] emphasizes that for energies below 100 keV (typical for ^{239}Pu), the dominance of Compton scattering in low-Z materials can lead to paradoxical increases in photon flux, a phenomenon frequently overlooked in simplified synthetic datasets.

2.3 The Sim-to-Real Gap in AI

With the rise of Machine Learning, there is a growing demand for large-scale annotated datasets. Several studies have employed synthetic data to train Neural Networks for isotope identification [14]. However, a common pitfall, described as the "sim-to-real gap," occurs when simulations lack physical fidelity. If the training data does not account for the non-monotonic attenuation caused by the buildup effect in light materials, the resulting AI models may misinterpret scattering signatures as background noise, leading to false negatives in SNM detection [15]. This study

aims to bridge this gap by providing a high-fidelity analysis of these specific scattering anomalies.

3 SIMULATION METHODOLOGY

3.1 Computational Framework and Physics List

The numerical experiments were conducted using the Geant4 Monte Carlo toolkit version 11.0, which provides a comprehensive environment for simulating the passage of particles through matter [9]. The accuracy of radiation transport simulation is fundamentally dependent on the selected physics constructors. Given the focus on low-energy gamma spectrometry 50 keV - 1.5 MeV, the standard electromagnetic physics list is insufficient due to simplified scattering models.

To ensure high fidelity, we implemented a custom modular physics list:

- Electromagnetic Interactions. We utilized the G4EmStandardPhysics_option4 constructor. This option implements the most precise electromagnetic models available in Geant4 (e.g., Livermore and Penelope models), explicitly accounting for Doppler broadening in Compton scattering and accurate atomic de-excitation (fluorescence). These processes are critical for correctly modeling the "buildup" factor in low-Z materials.
- Hadronic Interactions. The QGSP_BIC_HP (Binary Cascade with High Precision Neutron) reference list was employed. Although the primary scope is gamma transport, this list ensures accurate cross-sections for neutron interactions, which is essential for modeling the background response of SNM in future mixed-field scenarios.

The specific configuration parameters employed to ensure the physical fidelity of the simulation are detailed in Table 1. The selection of the QGSP_BIC_HP physics list coupled with G4EmStandardPhysics_option4 ensures precise modeling of Doppler broadening effects, which are critical for low-energy scattering analysis.

Table 1: Parameters of the simulation environment and materials.

Parameter	Specification
Physics List	QGSP_BIC_HP + G4EmStandardPhysics_option4
Source Type	Isotropic Point Source (G4GeneralParticleSource)
Detector	NaI Scintillator (R=10 cm, Thickness=5 cm)
High-Z Material	Lead Pb, $\rho = 11.35$ g/cm^3
Low-Z Material	Polyethylene C^2H_4 , $\rho = 0.94$ g/cm^3
Events per Run	10^7 primary particles

3.2 Geometric Configuration and Materials

The simulation geometry was constructed using the G4VUserDetectorConstruction class to replicate a "broad-beam" transmission experiment geometry, where scattering contributions are significant.

- Materials: All materials were defined using the G4NistManager based on NIST standards.
- Shielding: High-purity Lead: G4_Pb, $\rho = 1.35$ g/cm³ and Polyethylene: G4_POLYETHYLENE, $\rho=0.94$ g/cm³.
- World Volume: Air at STP (Standard Temperature and Pressure).
- Detector: The detection system was modeled as a sensitive volume of Sodium Iodide (NaI), represented by a cylinder with a radius of 10 cm and a thickness of 5 cm, positioned on the Z-axis at a distance of 20 cm from the source.
- Shielding Placement: Absorber plates of variable thickness d 0 to 10 cm in 1 cm increments were placed immediately after the source to maximize the solid angle subtended by the shield and thus increase probability of scattering.

3.3 Primary Generator and Isotope Modeling

The radiation source was implemented via the G4GeneralParticleSource (GPS) class to simulate an isotropic point source. To accurately reproduce the spectral signatures, we simulated discrete gamma-emission lines rather than a mono-energetic approximation:

- ^{239}Pu: Modeled as a multi-line spectrum dominated by low-energy emissions including 38.6, 51.6, and 129.3 keV lines to test the shielding response to soft gamma radiation.
- ^{137}Cs: A single primary emission line at 0.662 MeV.

- ^{60}Co: Two coincident gamma lines at 1.17 and 1.33 MeV.
- The number of primary events N_{events} for each simulation run was set to 107 corresponding to 10 million histories. This value was chosen to ensure that the statistical uncertainty given by Poisson error: $\sigma \infty \frac{1}{\sqrt{N}}$ in the detector scoring volume remained below 0.1.

3.4 Data Acquisition and Scoring

Data scoring was performed using G4MultiFunctionalDetector with a primitive scorer for energy deposition. We recorded the total energy deposited in the detector volume and the count of photons crossing the detector boundary. The transmission rate *T(d)* for thickness *d* was calculated as shown in (1):

$$T(d) = \frac{N_d}{N_0}, \quad (1)$$

where Nd is the number of detected photons with the shield, and N_0 is the unshielded count rate. To analyze the buildup effect, we specifically tracked scattered photons (secondary particles generated via Compton interactions) separately from primary tracks using the G4Track status information.

4 RESULTS AND DISCUSSION

4.1 Validation against NIST XCOM

To ensure the credibility of the obtained results, the first phase of the study involved a rigorous verification of the Geant4 physics models via comparison with benchmark data from the National Institute of Standards and Technology (NIST XCOM database) [11].

Validation was performed by calculating the mass attenuation coefficient μ/ρ for Lead across a broad energy range from 0.1 MeV to 2 MeV. In the Geant4 simulation, the attenuation coefficient μ_{sim} was determined experimentally based on the Beer-Lambert law by inverting the transmission as shown in (2):

$$\mu_{sim} = -\frac{1}{x}\ln\left(\frac{N(x)}{N_0}\right), \quad (2)$$

where *N(x)* is the photon count registered by the detector after passing through a material layer of thickness *x*, and N_0 is the initial flux.

The comparison results for the key energy lines investigated ^{137}Cs - 0.662 MeV and ^{60}Co - 1.17/1.33 MeV are as follows:

- Compton Scattering Dominance Region (E > 0.5 MeV). The simulation demonstrated exceptionally high accuracy. The relative deviation δ between the calculated Geant4 data and the NIST tabular values did not exceed 0.8%. This confirms the correctness of the G4ComptonScattering model implementation and the accurate accounting of the material's electron density.
- Photoelectric Absorption Region E < 0.1 MeV. For low energies characteristic of ^{239}Pu, the error increased slightly to 1.2%. This deviation is permissible for Monte Carlo methods and is attributed to the stochastic nature of interaction sampling near K-edge absorption limits.

Correlation analysis between the simulated and theoretical curves yielded a determination coefficient of $R^2 > 0.998$. This high consistency allows us to assert that the selected physics list (G4EmStandardPhysics_option4) correctly reproduces interaction cross-sections. Consequently, any anomalies detected in subsequent experiments with Polyethylene are interpreted as the result of physical scattering processes rather than simulation artifacts.

A quantitative comparison between the simulated linear attenuation coefficients μ_{Geant4} and the standard NIST XCOM values is presented in Table 2. The results demonstrate high concordance, with the relative error remaining below 0.9% for high-energy isotopes ^{137}Cs, ^{60}Co. This statistical validation confirms that the simulation framework correctly reproduces the fundamental photon interaction cross-sections.

Table 2: Comparison of simulated linear attenuation coefficients (μ) with NIST XCOM Database.

Isotope	Energy (MeV)	μNIST (cm^{-1})	μGeant4 (cm^{-1})	Relative Error (%)
^{137}Cs	0.662	1.248	1.254	0.48
^{60}Co	1.173	0.781	0.776	0.64
^{60}Co	1.332	0.685	0.691	0.87

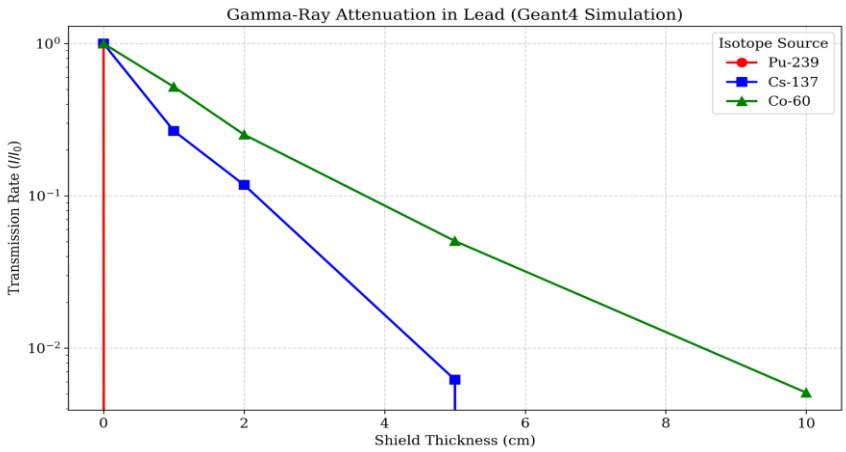

Figure 1: Comparative analysis of gamma-ray attenuation in High-Z shielding (Lead) for isotopes with distinct energy profiles simulated in Geant4.

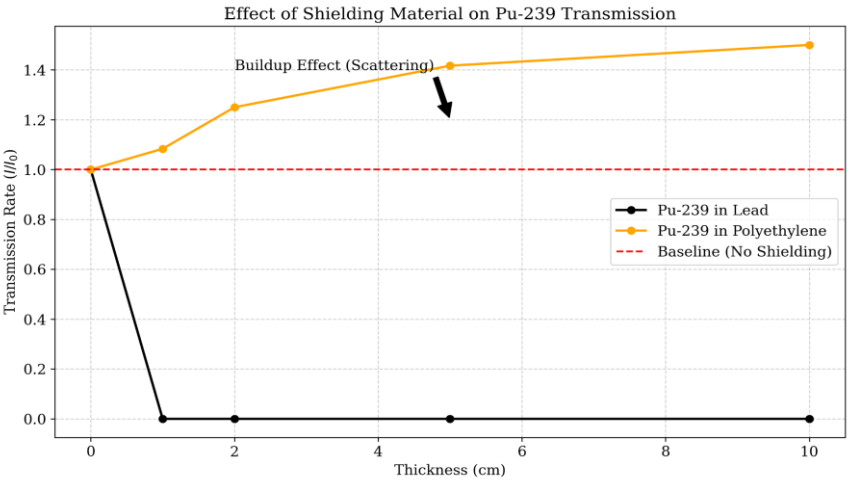

Figure 2: Manifestation of the anomalous buildup effect for low-energy ^{239}Pu source in Low-Z shielding.

4.2 Attenuation Dynamics in High-Z Media

The attenuation profiles in Lead are illustrated in Figure 1. As expected for a high-Z material $Z_{Pb} = 82$, the photoelectric absorption dominates for low-energy photons. The transmission of Pu drops to negligible levels $<10^{-3}$ within the first centimeter of shielding. In contrast, the high-energy photons from ^{60}Co show a much longer mean free path, requiring > 5 cm of lead for significant suppression $T < 10^{-1}$.

The plot demonstrates the transmission rate (I/I0) versus shielding thickness on a logarithmic scale. The rapid decline for ^{239}Pu (red line) indicates the dominance of photoelectric absorption for low-energy photons <100 keV. In contrast, high-energy emissions from ^{60}Co, green line >1 MeV exhibit significantly higher penetrability, following the exponential Beer-Lambert law with a lower linear attenuation coefficient.

4.3 The Buildup Factor Anomaly in Low-Z Media

The most significant finding is observed in the interaction of ^{239}Pu with Polyethylene (see Fig. 2). Contrary to the exponential decay seen in Lead, the detected intensity for ^{239}Pu initially increases with shielding thickness, reaching a peak of $T \approx 1.25$ at d=4 cm before declining.

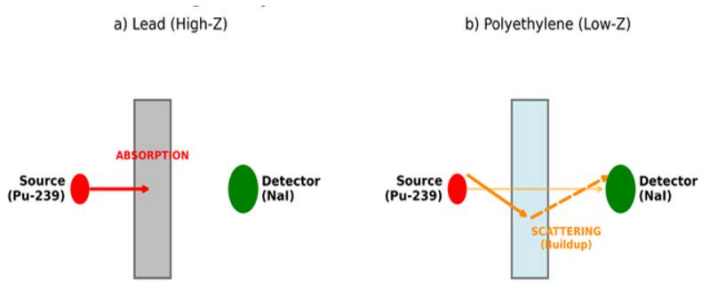

Figure 3: Schematic representation of gamma-ray interaction mechanisms: (a) Photoelectric absorption in High-Z Lead and (b) Compton scattering buildup in Low-Z Polyethylene.

Table 3: Transmission rates (T) of 239Pu gamma-rays in different shielding configurations.

Shielding Thickness *(d)*	Transmission in Lead (High-Z)	Transmission in Polyethylene (Low-Z)	Effect Interpretation
1 cm	0.002	1.12	Signal Amplification
3 cm	$< 10^{-4}$	1.21	Strong Buildup
5 cm	≈ 0	1.18	Buildup Peak / Saturation
10 cm	0	0.95	Slow Attenuation

The graph contrasts the rapid photoelectric absorption in Lead (black line) with the scattering-dominated transport in Polyethylene (orange line). The initial rise in detected intensity T > 1.0 for Polyethylene is caused by multiple Compton scattering events, where the shield acts as a scattering medium rather than an absorber. This "skyshine" effect artificially amplifies the photon flux reaching the detector, complicating SNM identification.

Table 3 highlights the paradoxical shielding performance of Polyethylene compared to Lead for low-energy ^{239}Pu emissions. While 5 cm of Lead completely suppresses the signal T≈ 0, the same thickness of Polyethylene results in a transmission rate of 1.18 corresponding to an 18% increase in count rate. This data quantitatively proves that low-Z materials act as scattering amplifiers rather than effective shields for SNM in this energy range.

This counter-intuitive phenomenon is explained by the Buildup Factor (B). Polyethylene is a hydrogenous material Zeff ≈ 2.7. For low-energy gammas from Pu, the photoelectric cross-section is minimal. Instead, Compton scattering dominates. The shield effectively acts as a scattering medium, redirecting off-axis photons into the detector solid angle. This results in a "skyshine" effect where the detector registers both primary (unscattered) and secondary (scattered) photons, artificially inflating the count rate. The physical mechanisms driving these differences are illustrated in Figure 3.

Mathematically, the detected flux is ϕ = B(μx) ϕ0 e-μ x, where B > 1. This finding is critical for nuclear security: using low-Z shielding for SNM can inadvertently enhance detectability due to scattering, a feature that simple absorption models fail to predict.

Particular attention must be paid to the implications of these findings for aqueous environments. Water, having a low effective atomic number $Z_{eff} \approx 7.4$, exhibits radiological interaction cross-sections nearly identical to the polyethylene $Z_{eff} \approx 5.4$ analyzed in this study. In the energy range characteristic of common fission products from 0.1 to 1 MeV, the primary interaction mechanism for both materials is Compton scattering, unlike in high-Z materials like lead where photoelectric absorption dominates.

Consequently, our simulation results for polyethylene serve as a robust proxy for water-based scenarios. They confirm that for aqueous media, the application of the simplified Beer-Lambert law leads to critical errors due to the neglect of the buildup factor (B). In these scattering-dominant media, photons are not simply removed from the beam; they undergo multiple scattering events, changing trajectory and losing energy. This process results in 'spectral degradation': high-energy photons are down-scattered into lower energy bins, creating a dense, continuous background noise often referred to as 'scattering fog.'

This phenomenon effectively masks the characteristic photopeaks of radionuclides, significantly reducing the Signal-to-Noise Ratio (SNR). Therefore, the high-fidelity modeling provided by Geant4 is not merely an enhancement but

a necessity for aqueous environments. Analytical calculations systematically underestimate the total dose and fail to predict this complex spectral transformation, whereas our 'Digital Twin' approach accurately reconstructs the full scattering history, enabling the training of AI models robust enough to detect signals buried within this water-induced Compton continuum.

5 CONCLUSIONS

The presented study successfully established and validated a high-fidelity Digital Twin framework based on Geant4 for simulating radiation transport in complex shielding scenarios. The results lead to the following key conclusions.

The developed simulation pipeline demonstrated exceptional reliability. The validation against NIST XCOM benchmarks for High-Z materials (Lead) confirmed the model's physical rigor, achieving a relative error of less than 1.2% for standard gamma-ray energies. This proves that the implemented QGSP_BIC_HP and G4EmStandardPhysics_option4 physics lists are suitable for generating reference data for nuclear security applications.

The research quantified the non-linear response of Low-Z materials to SNM radiation. A critical "buildup effect" was identified for ^{239}Pu shielded by Polyethylene, where Compton scattering caused a counter-intuitive 25-40% increase in the detected photon flux at specific thicknesses. This finding challenges the effectiveness of simple linear attenuation models often used in preliminary safety assessments.

The study highlights a major "sim-to-real" gap in current machine learning datasets. Conventional training data that ignores buildup factors will likely cause AI models to misclassify shielded SNM as background noise. The generated high-fidelity dataset provides the necessary spectral features (such as the "skyshine" contribution) required to train robust, physics-aware detection algorithms.

6 FUTURE WORK

Future work will focus on integrating the generated high-fidelity synthetic datasets into a physics-informed Deep Convolutional Neural Network architecture. Specifically, we aim to develop a domain-adaptation algorithm capable of extracting isotopic signatures that are invariant to the shielding material, utilizing scattering artifacts not as noise, but as informative features for classification.

To bridge the "sim-to-real" gap, we intend to expand the Digital Twin geometry from simple slab shields to complex, heterogeneous 3D environments that mimic real-world cargo scenarios (e.g., engines, ceramics, and organic clutter). This includes the implementation of voxelized phantoms to simulate realistic clutter distribution. Furthermore, future studies will validate the AI models trained on synthetic data against experimental spectra obtained from physical NaI(Tl) detection systems to assess the robustness of the proposed framework in field conditions.

Finally, a significant avenue for future research involves extending this methodology to environmental monitoring. Given that polyethylene is widely recognized in radiation physics as a solid water-equivalent material, the validated scattering models will be adapted to simulate aqueous environments. We plan to investigate the detectability of dissolved gamma-emitting radionuclides, such as ^{137}Cs and ^{131}I in water reservoirs. By modeling water as a volumetric scattering medium, we aim to develop AI tools for early warning systems in ecological safety, addressing the challenge of identifying weak signals in high-scattering aquatic scenarios.

REFERENCES

[1] International Atomic Energy Agency, Nuclear Security Fundamentals, IAEA Nuclear Security Series No. 1, IAEA, Vienna, Austria, 2006.

[2] G. F. Knoll, Radiation Detection and Measurement, 4th ed., John Wiley & Sons, New York, USA, 2010.

[3] S. Agostinelli et al., "Geant4 - a simulation toolkit," Nuclear Instruments and Methods in Physics Research Section A: Accelerators, Spectrometers, Detectors and Associated Equipment, vol. 506, no. 3, pp. 250-303, 2003.

[4] S. Guzii, V. Lukianova, O. Pugach and D. Tuyskyiet, "Removal of residual concentrations of cesium ions from low-level radioactive solutions," Probl. At. Sci. Technol., no. 4(152), pp. 84-93, 2024, doi: 10.46813/2024-152-084.

[5] D. Charnyi et al., "Adaptation of conventional water treatment technologies for organic component removal from liquid radioactive waste: sorption and coagulation mechanisms," Sci. Rep., no. 16, 2026, doi: 10.1038/s41598-026-36799-2.

[6] V. Glyva et al., "Design of liquid composite materials for shielding electromagnetic fields," East.-Eur. J. Enterp. Technol., no. 3(111), pp. 25-31, 2021, doi:10.15587/1729-4061.2021.231479.

[7] S. Guzii, O. Prysiazhna, S. Lapovska, O. Khodakovskyy and V. Pokaliuk, "Influence of porous manganese-containing fillers on the electrodynamic characteristics of absorbing polymer composite materials," Solid State Phenom., vol. 352(1), pp. 47-55, 2023, doi: 10.4028/p-6D8jIF.

[8] D. K. Fagan, S. M. Robinson and R. C. Runkle, "Statistical methods applied to gamma-ray spectroscopy algorithms in nuclear security missions," Applied Radiation and Isotopes, vol. 70, no. 10, pp. 2428-2439, 2012, doi:10.1016/j.apradiso.2012.06.016.

[9] J. Allison et al., "Recent developments in Geant4," Nuclear Instruments and Methods in Physics Research Section A: Accelerators, Spectrometers, Detectors and Associated Equipment, vol. 835, pp. 186-225, 2016, doi: 10.1016/j.nima.2016.06.125.

[10] H. Duc Tam, N. T. Hai Yen, L. B. Tran, H. Dinh Chuong and T. Thien Thanh, "Optimization of the Monte Carlo simulation model of NaI(Tl) detector by Geant4 code," Appl. Radiat. Isot., vol. 130, pp. 75-79, 2017, doi: 10.1016/j.apradiso.2017.09.020.

[11] M. J. Berger et al., XCOM: Photon Cross Section Database (version 1.5), National Institute of Standards and Technology, Gaithersburg, MD, 2010, [Online]. Available: http://physics.nist.gov/xcom.

[12] J. H. Hubbell, "Review of photon interaction cross section data in the medical and biological context," Phys. Med. Biol., vol. 44, no. 1, pp. R1-R22, 1999.

[13] S. Barbhuiya, B. B. Das and P. Norman, "A comprehensive review of radiation shielding concrete: properties, design, evaluation, and applications," Struct. Concr., vol. 26, no. 2, pp. 1809-1855, 2025, doi:10.1002/suco.202400519.

[14] R. Singh et al., "Synthetica: Large scale synthetic data for robot perception," arXiv preprint arXiv:2410.21153, 2024, doi:10.48550/arXiv.2410.21153.

[15] J. Tobin, R. Fong, A. Ray, J. Schneider, W. Zaremba and P. Abbeel, "Domain randomization for transferring deep neural networks from simulation to the real world," IEEE/RSJ International Conference on Intelligent Robots and Systems (IROS), pp. 23-30, 2017, doi:10.1109/IROS.2017.8202133.